geosciences

MDPI

Article

Thermal and Fluid Evolution of Paleozoic Rocks in the Sakmara Zone and Eastern Pre-Caspian Basin, Western Kazakhstan

Talgat Yensepbayev [1,*], Ismail Kuandykov [1], Alina Abdrassil [1], Jean-Jacques Royer [2], Michel Cathelineau [2] and Lyaila Nurmaganbetova [1]

[1] KazNITU, Satbayev University, 050013 Almaty, Kazakhstan; i.kuandykov@satbayev.university (I.K.); a.abdrassil@satbayev.university (A.A.); lnurmaganbetova@gmail.com (L.N.)
[2] Université de Lorraine, CNRS, GeoRessources, 54000 Nancy, France; jean.jacques.royer@gmail.com (J.-J.R.)
* Correspondence: t.yensepbayev@satbayev.university; Tel.: +7-777-693-2244

Abstract

Understanding the thermal evolution of foreland basins is essential for reconstructing hydrocarbon generation, migration, and accumulation, and for improving petroleum-system models in thrust-influenced foreland basins worldwide, including the Pre-Uralian Foredeep. However, the thermal regime of Paleozoic formations along the eastern margin of the Pre-Caspian Basin remains poorly constrained, particularly with respect to the relative roles of burial heating and tectonically driven hydrothermal circulation. This study investigates the thermal history and petroleum implications of calcite-hosted fluid inclusions in fractures and veins within Upper Silurian to Lower Permian sedimentary rocks of the Sakmara accretionary zone (Mugodzhar, Southern Urals), the Pre-Uralian Foredeep, and the eastern Pre-Caspian Basin, western Kazakhstan. Aqueous fluid inclusions yield homogenization temperatures ranging from ~50 to 280 °C and define several fluid populations. The dominant population (Th ≈ 87–146 °C) is interpreted as burial-related, whereas low-temperature inclusions (50–78 °C) reflect early diagenetic and/or late-stage fluid circulation. Higher-temperature inclusions (>180 °C) record transient hydrothermal events associated with fault-controlled fluid flow. These results indicate that the basin's thermal evolution was governed by the combined effects of burial heating and episodic hydrothermal activity. Comparison with available Rock–Eval, vitrinite reflectance, molecular maturity, and burial-history data suggests that the sampled Paleozoic formations were generally immature to marginally mature, whereas hydrocarbons were likely generated in deeper or adjacent, more mature zones (>4 km) and subsequently migrated into the studied units. The results provide a regional framework for understanding fluid-flow and thermal processes in the Uralian foreland system and demonstrate the broader value of integrating fluid-inclusion microthermometry with structural and burial-history analyses to reconstruct basin evolution and hydrocarbon migration in foreland basins worldwide.

Keywords: fluid inclusions; Southern Urals; thermal maturity; hydrothermal activity; burial diagenesis; fault-controlled fluid circulation; orogen-foreland systems; low geothermal gradient

Academic Editor: Simona Ferrando

Received: 4 May 2026
Revised: 19 June 2026
Accepted: 23 June 2026
Published: 1 July 2026

1. Introduction

Reconstructing the thermal and fluid evolution of sedimentary basins and collisional belts is essential for understanding burial history, diagenesis, hydrothermal circulation, and petroleum-system evolution [1,2]. Similar tectono-thermal processes have been documented in major foreland and collisional basins worldwide, including the Appalachian

 https://doi.org/10.3390/geosciences16070260

Basin [3], Western Canada Sedimentary Basin [4], Congo Basin [5], Zagros Basin [6], Alpine foreland basins [7], and the South Caspian Basin [8], where burial heating and fault-controlled hydrothermal circulation significantly influenced reservoir diagenesis and hydrocarbon migration. In many carbonate reservoirs, porosity evolution reflects the interplay between diagenetic enhancement (dolomitization, dissolution, and fracturing) and reduction (cementation and compaction). Tectonic fracture networks facilitated fluid migration and reservoir connectivity, whereas isotopic evidence indicates circulation of mixed marine and meteoric fluids during shallow-burial diagenesis [9]. Fluid inclusions (FI) in carbonate minerals provide direct constraints on paleotemperatures, fluid salinity, and pressure–temperature (P–T) conditions during mineral precipitation and fracture sealing, although they do not necessarily record the complete thermal history of the host rocks. In foreland basins and accretionary–collisional settings, FI records commonly reflect a combination of burial heating and transient hydrothermal events driven by fault-controlled advective heat transfer [6–12].

The Pre-Uralian Foredeep and the Sakmara zone (Mugodzhar segment, Southern Urals) form a classic Late Paleozoic foreland basin–accretionary system that developed during the transition from oceanic subduction to continental collision [13–19]. Geological evidence indicates burial depths of ~2–4 km for Paleozoic sediments, corresponding to low (~20 °C/km) to moderate (~40 °C/km) conductive geothermal gradients. However, fluid inclusions in carbonate veins locally record elevated homogenization temperatures, suggesting transient thermal anomalies associated with advective heat transfer. These tectonic, thermal, and fluid-flow processes strongly influenced sedimentary evolution and petroleum systems, particularly where Upper Devonian–Carboniferous basinal sediments interfinger with reservoir units, occur adjacent to organic-rich shales, and facilitate vertical hydrocarbon migration along major fault systems [13,16,17].

To better constrain these processes, this study integrates new and published microthermometric data from aqueous fluid inclusions (FI) in Silurian–Permian limestones and litharenites of the Pre-Caspian Basin, Pre-Uralian Foredeep, and Sakmara zone with regional geological and structural constraints. The objectives are to: (i) evaluate fluid-related thermal regimes recorded by FI and compare them with independently constrained burial conditions and available regional maturity data; (ii) characterize low-temperature FI populations (Th = 50–78 °C); (iii) assess high-temperature FI populations as indicators of hydrothermal pulses; and (iv) propose a conceptual P–T–t model. The results provide insights applicable to other orogen–foreland systems affected by transient hydrothermal fluid circulation.

2. Geological Setting

The study area is located along the eastern margin of the Pre-Caspian Basin and includes the adjacent Pre-Uralian Foredeep and the Mugodzhar segment of the Southern Urals in western Kazakhstan (Figure 1A,B). During the Late Paleozoic, this region formed a foreland-accretionary system between the Uralian orogen to the east and the Pre-Caspian Basin to the west. The principal tectonic units are the Sakmara accretionary zone, the Pre-Uralian Foredeep, and the eastern margin of the Pre-Caspian Basin. At present, the eastern flank of the basin is marked by the Temir and Zharkamys uplifts, which host the region's main oil and gas fields.

The studied fluid inclusions occur in Silurian–Permian carbonate and siliciclastic sedimentary successions within these units. The regional geological framework, major fault systems, and thrust architecture (Figure 1A,B) provide the basis for interpreting the thermal and fluid evolution discussed below.

2.1. Tectonic Evolution

The Sakmara accretionary zone is a major tectonostratigraphic unit along the western flank of the Southern Urals and its southern continuation into the Mugodzhar region (Figure 3). It forms an accretionary-thrust complex that formed during the closure of the Uralian Ocean along the eastern margin of the East European continent [14–22].

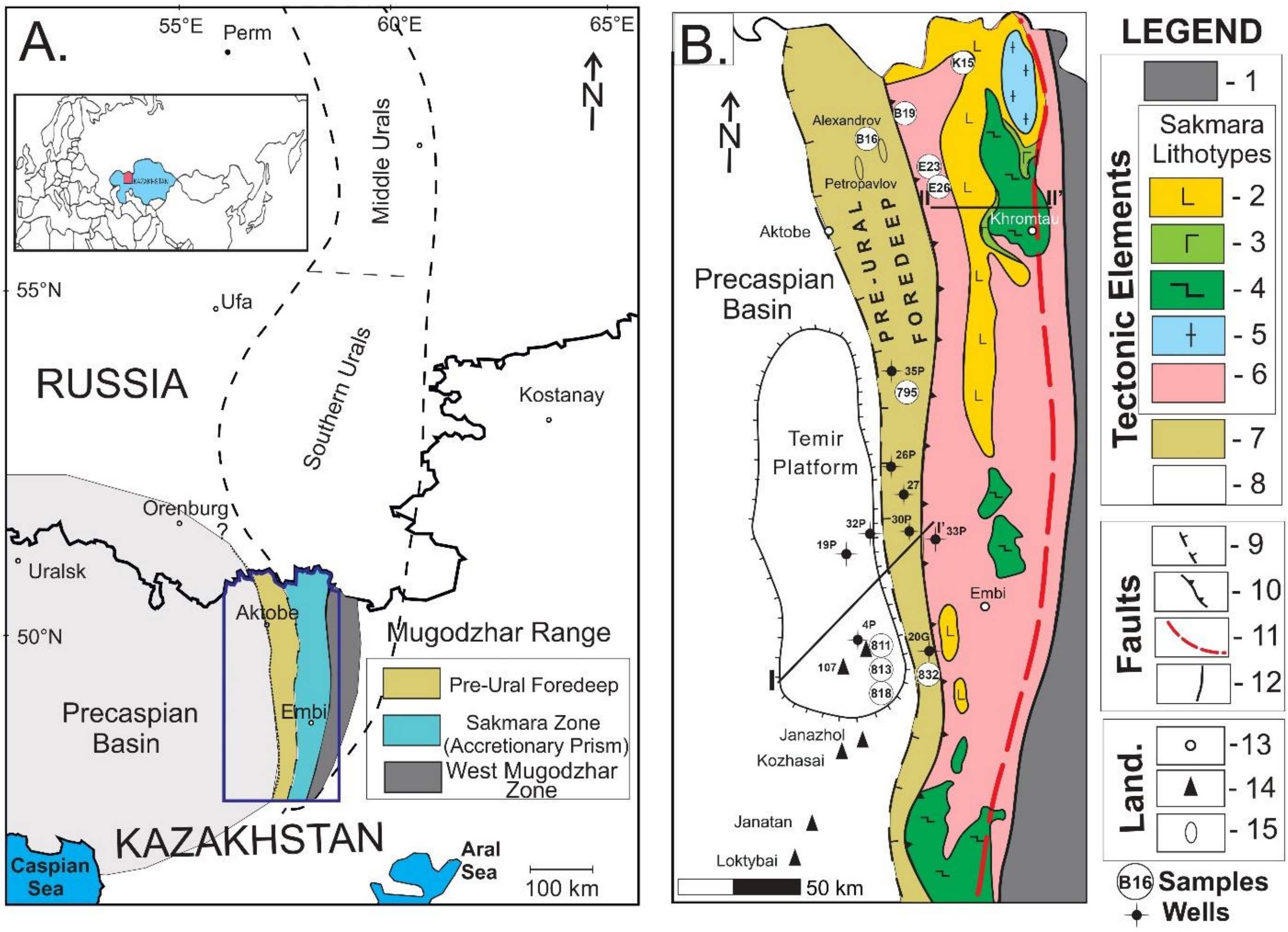

Figure 1. (**A**) Regional overview of the Uralian orogenic belt, showing the Middle and Southern Urals and their southern continuation into the Mugodzhar region. The dark blue rectangle outlines the study area and the tectonic map presented in Figure 1B. The Sakmara zone is highlighted in light blue, and the solid line within it marks the Main Uralian Fault. (**B**) Tectonic map of the eastern Pre-Caspian Basin, the Pre-Uralian Foredeep, and the Sakmara zone of the Mugodzhar Range. The map shows the structural framework, major thrust systems, and regional fault network controlling deformation and basin evolution (modified after [23,24]). Legend. 1—West Mugodzhar Zone; 2—Effusive rocks; 3—Gabbro intrusions; 4—Ultramafic rocks; 5—Gneisses and crystalline rocks; 6—Sedimentary-volcaniclastic rocks of the Sakmara zone; 7—Pre-Uralian Foredeep; 8—Pre-Caspian Basin; 9—Ashchisay Fault; 10—Sakmara–Kokpekty Thrust Fault; 11—Main Uralian Fault; 12—West Mugodzhar Fault; 13—Cities; 14—Oil and gas fields; 15—Circled numbers indicate the studied samples.

Its evolution records a transition from Early Paleozoic rifting and oceanic spreading to Devonian subduction and island-arc magmatism, followed by Late Devonian–Permian accretion and continental collision [19,21–23].

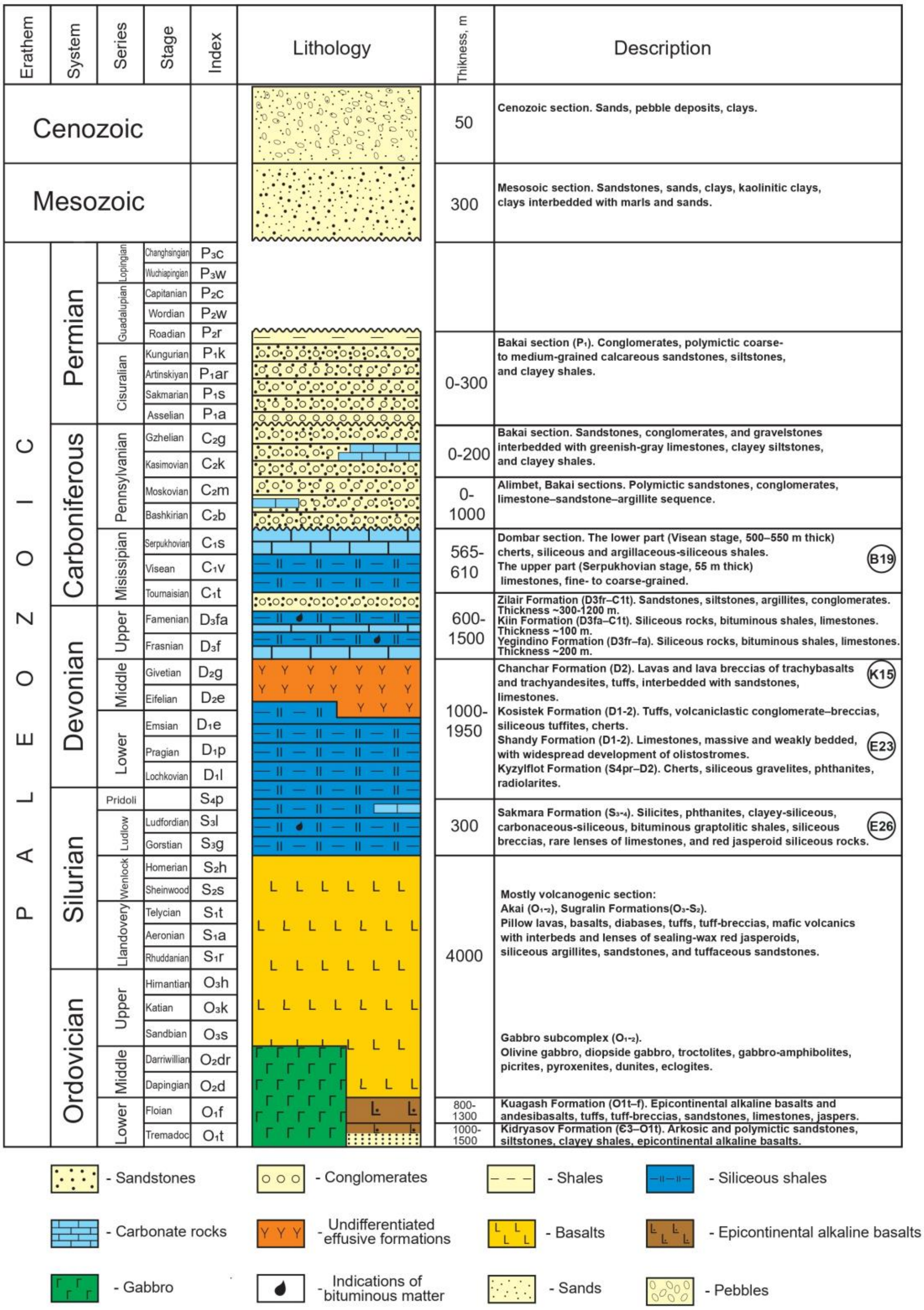

Figure 2. Generalized lithostratigraphic column of the Sakmara zone (Mugodzhar segment, Southern Urals), showing the stratigraphic succession and principal lithologies (modified from [19–30]).

Early extensional stages are represented by Ordovician alkaline volcanic rocks and associated terrigenous sediments of the Kidryasov and Kuagash formations [15,19,21,25–28], whereas oceanic spreading is recorded by pillow basalts of the Akai and Sugralin formations [15,18,19,23,26,29]. Continued basin development is documented by Silurian volcanic and siliceous successions of the Sugralin and Sakmara formations [19,21,22,30].

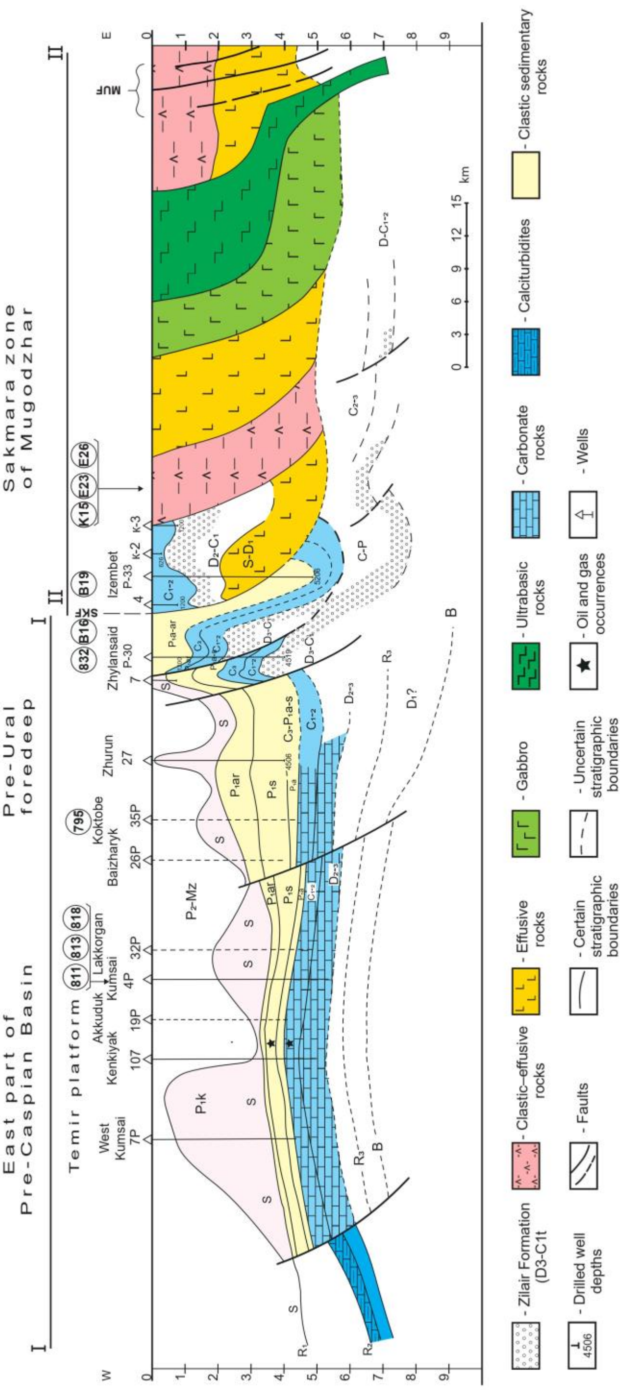

Figure 3. Geological cross-section across the eastern Pre-Caspian Basin, the Pre-Uralian Foredeep, and the Sakmara zone of the Mugodzhar segment. The section illustrates the thrust architecture, stratigraphic relationships, and inferred burial depths of Silurian–Carboniferous units hosting the studied fluid inclusions. Major fault zones, including the Sakmara–Kokpekty Thrust and the Main Uralian Fault, are interpreted as potential pathways for focused fluid flow and advective heat transport (modified after [23–30]). Legend. Stratigraphic units: P_2-Mz—Clastic deposits; P_1k—Salts; P_1ar—Clastic deposits; P_1s—Clastic deposits; P_1a—Carbonate–clastic deposits; P_1a-s—Carbonate–clastic deposits; P_1a-ar—Clastic deposits; C-P—Carbonate-clastic deposits; C_3-P_1a-s—Carbonate–clastic deposits; C_3. Carbonate–clastic deposits; $C_{2–3}$—Carbonate-clastic rocks; $C_{1–2}$—Carbonate rocks; D_3-C_1—Carbonate–clastic deposits; D-$C_{1–2}$—Carbonate-clastic deposits; $D_{2–3}$—Carbonate–clastic deposits; S-D_1—Volcanic rocks. Other symbols: R_1, R_2, R_3, B—Seismic reflectors; SKF—Sakmara-Kokpektian Fault; MUF—Main Uralian Fault.

A major geodynamic reorganization occurred during the Devonian with the onset of subduction and island-arc magmatism, represented by the Chanchar, Kyzylflot, and Kosistek formations [14,15,18,19,23,26,29,30]. Progressive accretion of island arcs and the Mugodzhar microcontinent onto the eastern margin of the East European continent during the Late Devonian–Carboniferous led to the development of the Uralian orogen and the associated Pre-Uralian Foredeep [23,30–33]. Collision began during the Famennian, was largely completed by the Early Carboniferous, and was followed by renewed tectonic activity during the Late Carboniferous and Permian [19–21,34].

The resulting structural framework is characterized by thrust stacking and major fault systems, including the Sakmara–Kokpekty Thrust and the Main Uralian Fault. These structures strongly influenced basin evolution, fluid circulation, and heat transfer and therefore represent key controls on the thermal evolution investigated in this study.

2.2. Stratigraphy and Petroleum System Context

The studied fluid inclusions occur in Silurian–Permian sedimentary rocks deposited in platform, slope, basinal, and foredeep environments. Carbonate successions dominate the Devonian–Carboniferous platform domain of the eastern Pre-Caspian Basin, whereas siliciclastic and gravity-flow deposits become increasingly abundant in the Pre-Uralian Foredeep as a result of erosion of the growing Uralian orogen.

Maximum burial depths inferred from lithostratigraphic relationships and regional subsidence models range from approximately 1.8–2.4 km in the Alexandrov Fold to 3.7–4.5 km in the Sakmara Formation. These estimates provide an independent framework for evaluating the thermal significance of fluid-inclusion homogenization temperatures.

The Devonian-Carboniferous formations constitute important petroleum-system elements, including both potential source rocks and reservoir intervals. Porous sandstones of the Shandy Formation (D_{1-2}) and the Dombar Hills succession (Visean-Bachkirian) may serve as reservoir rocks, whereas the organic-rich siliceous and carbonate rocks and bituminous shales of the Yeguindy (Frasnian-Famennian) and Kiin (Famennian-Tournaisian) formations, deposited under euxinic conditions, represent potential source rocks and seals. Comparable facies also occur along the eastern margin of the Pre-Caspian Basin [24] (Figure 2). Together with the structural framework of the Sakmara thrust zone and the Pre-Uralian Foredeep, these units provide the geological context for interpreting the fluid-inclusion record and its implications for basin evolution and hydrocarbon migration [35].

2.3. Geodynamic Controls on Thermal Regime and Fluid Circulation

Interpretation of the fluid-inclusion record requires consideration of both burial history and tectonic evolution. Burial-depth estimates derived from stratigraphic reconstructions provide first-order constraints on pressure–temperature conditions during fluid entrapment. However, the Devonian–Carboniferous transition from subduction to collision was accompanied by significant changes in heat flow and crustal permeability.

The development of deep-seated faults, thrusts, and fracture networks likely promoted focused fluid circulation and advective heat transfer. Devonian magmatism and subsequent tectonic reactivation may have locally enhanced heat flow and facilitated the ascent of hydrothermal fluids. Similar processes have been documented in collisional and post-subduction settings worldwide, where major fault zones act as conduits for fluid flow and heat transport [36–39].

Following the collision, continued uplift and tectonic reactivation further increased permeability, facilitating the circulation of meteoric and formation waters, particularly within the frontal thrust belt. These conditions favored open hydrogeological systems and fluid pressures close to hydrostatic values in many carbonate-hosted fracture systems.

Because fault zones commonly act as preferential pathways for fluid flow and heat redistribution [36–41], the homogenization temperatures recorded by fluid inclusions likely reflect a combination of burial heating and episodic fault-controlled hydrothermal circulation. This framework provides the basis for evaluating the relative contributions of conductive and advective heat transfer to the thermal evolution of the Sakmara zone, the Pre-Uralian Foredeep, and the eastern Pre-Caspian Basin.

Several factors may have contributed to locally elevated geothermal gradients, including Devonian volcanism and its residual thermal effects into the Carboniferous, as well as the development of deep-seated faults and fracture networks during subduction and collision, particularly along thrust fronts. These structures likely acted as conduits for ascending hydrothermal fluids and advective heat transfer, generating transient thermal anomalies above regional background conditions.

Enhanced heat flow and hydrothermal circulation are well documented in collisional and post-subduction settings, where increased permeability along faults and thrusts promotes focused fluid flow and advective heat transport [36–39]. Because fault zones commonly exhibit much higher permeability than the surrounding host rocks, they act as preferential pathways for hydrothermal fluids and exert a major control on heat redistribution and fluid migration [36–41].

The tectonic position of the Sakmara zone within an accretionary–collisional belt (Figure 1A), together with the stratigraphic architecture of the carbonate-bearing successions (Figure 1B) and the thrust-dominated structural framework, suggests that the observed homogenization temperatures cannot be explained solely by steady-state conductive geothermal gradients. Deep-seated faults and thrust systems likely acted as conduits for fluid flow and advective heat transfer, generating transient thermal anomalies recorded by fluid inclusions. The geological and facies characteristics of the studied samples, together with their fluid-inclusion types, are summarized in Table 1.

Table 1. Geological and facies characteristics of the studied samples and associated fluid inclusion types [1].

No.	Locality/Well	Depth (m)	Formation Age	Paléo-Environment	Facies
818	Kumsai 4P	4479–4494	C_2b	Middle platform	Biomicrite packstone
813	Kumsai 4P	5429–5442	D_2g–D_3fr	Core reef/back-reef transition	Biomicrite–wackestone with stromatoporoids
811	Kumsai 4P	5638–5648	D_2–D_3	Inner platform	Biomicrosparite–packstone
832	Karnak 20G	2195–2200	P_1as	Slope with turbidites	Litharenite
795	Koktobe 35P	3993–3998	P_1s	Slope with turbidites	Litharenite
B16	Alexandrov Fold	Quarry	P_1	Sabkha–lagoon system	Halite-bearing limestone
B19	Dombar area	Outcrop	C_1v-s	Middle platform	Biomicrite-packstone
K15	Chanchar Fm	Outcrop	D_2	Platform	Recrystallized limestone
E23	Shandy Fm	Outcrop	$D_{1–2}$	Platform	Recrystallized limestone
E26	Sakmara Fm	Outcrop	$S_{3–4}$	External platform	Biomicrite-packstone

[1] All inclusions are Lw-type (aqueous biphasic) in calcite filling host fractures, except sample K15, which contains both fracture- and vein-hosted calcite. Notes: Well depths are measured depths; outcrop samples were collected at the surface.

https://doi.org/10.3390/geosciences16070260

3. Materials and Methods

3.1. Sampling and Petrography

Samples were collected from outcrops, quarries, and wells within the Sakmara accretionary zone (outcrops), the Pre-Uralian Basin (Alexandrov fold outcrop; Koktobe and Karnak wells), and the Temir Platform of the Pre-Caspian Basin (Kumsai well).

Fluid inclusions in Silurian–Carboniferous sedimentary successions were investigated to refine interpretations of diagenetic and hydrothermal processes associated with burial and tectonic evolution. Inclusions occur mainly in calcite filling fractures, microfractures, and veins in carbonate rocks and, less commonly, in terrigenous rocks (litharenites). Volcanic and siliceous rocks were also examined, but no fluid inclusions suitable for microthermometric analysis were identified.

Doubly polished thick sections (100–150 μm) were prepared for petrographic and microthermometric analyses. Petrographic observations under transmitted and reflected light were used to identify suitable host minerals, primarily fracture- and vein-filling calcite, and to establish textural relationships between inclusions and host phases.

Ten representative samples were selected for detailed study, including core samples from subsalt Paleozoic successions of the Kumsai, Karnak, and Koktobe wells, and outcrop samples from the Alexandrov Fold, Dombar area, and the Chanchar, Shandy, and Sakmara formations. Sample selection was based on the presence of fractures and veins filled with diagenetic minerals, mainly calcite and locally quartz, suitable for fluid inclusion studies. In outcrop sections, 2–5 hand specimens were collected from each locality, preferentially from Paleozoic units displaying fracture- or vein-related mineralization. Core samples were selected from available subsalt Paleozoic intervals provided by operating companies.

The final dataset was chosen according to mineral-fill quality, fluid-inclusion preservation, and suitability for petrographic and microthermometric analyses. The geological setting, age, depositional environment, lithology, and fluid-inclusion characteristics of the studied samples are summarized in Table 1.

3.2. Fluid Inclusion Microthermometry

Fluid inclusion microthermometry was conducted on carbonate, terrigenous, siliceous, and volcanic rocks ranging from the Upper Silurian to the Lower Permian, collected from the eastern margin of the Pre-Caspian Basin, the Pre-Uralian Foredeep, and the Sakmara accretionary zone (Mugodzhar).

Fluid inclusions were examined petrographically to distinguish primary, pseudosecondary, and secondary aqueous inclusions hosted in calcite-filled fractures, microfractures, and veins.

Homogenization temperatures (Th) and final ice-melting temperatures (Tm) were measured for two-phase aqueous inclusions. Salinities were calculated as wt.% NaCl equivalents using standard H_2O–NaCl calibrations [42–46]. Only primary and pseudosecondary inclusions with consistent phase ratios were considered.

3.3. Salinity and Isochore Calculations

Salinities (wt.% NaCl equivalent) were calculated from final ice-melting temperatures using the polynomial equation of Bodnar (1993) for the H_2O–NaCl system [45]. This equation is valid for the low- to moderate-salinity aqueous inclusions observed in this study.

Isochores were calculated for representative fluid-inclusion populations using the H_2O–NaCl equation of state of Zhang and Frantz (1987) [42], implemented in a spreadsheet-based workflow.

https://doi.org/10.3390/geosciences16070260

Trapping conditions were estimated by intersecting isochores with independently constrained burial-depth ranges and first-order geothermal gradients derived from regional geological and heat-flow data. These estimates are interpreted as apparent P–T entrapment conditions rather than steady-state regional geothermal gradients. Geothermal gradients consistent with burial history and regional heat-flow constraints, assuming near-hydrostatic pressures [24], were considered the most likely for the studied sedimentary successions. Moderate overpressure conditions (up to ~1.4–1.8 times hydrostatic), particularly in the Pre-Caspian Basin, were also evaluated. These pressure variations have only a minor effect on the calculated trapping temperatures and do not alter the distinction between burial-related fluid-inclusion populations and higher-temperature populations interpreted as transient, advective hydrothermal events.

3.4. Analytical Procedure and Data Quality

Measurements were performed using a Linkam heating–freezing stage (Linkam Scientific Instruments Ltd., Tadworth, UK) mounted on a transmitted-light Zeiss Axio Scope.A1 microscope (Carl Zeiss Microscopy GmbH, Jena, Germany) whose website is (https://www.zeiss.com/microscopy/en/service-support.html, accessed on 22 June 2026). Analytical precision was ±0.1–0.2 °C for freezing measurements and ±1–2 °C for heating measurements. Only optically well-preserved, isolated two-phase inclusions were analyzed. Homogenization temperatures (Th) are interpreted as minimum trapping temperatures.

Apparent geothermal gradients, derived by relating Th values to independently constrained burial depths, are treated as first-order indicators of conductive versus advective thermal regimes rather than as steady-state geothermal gradients.

Microthermometric data for aqueous fluid inclusions are summarized in Table 2 and Figures 5–7. Several distinct Th–Tm populations were identified within individual samples, indicating multiple stages of fluid circulation.

Table 2. Microthermometric characteristics of aqueous biphasic fluid inclusions in calcite from different localities [1].

No.	Location Age	Sample No.	Population	Th (°C) min/max	Th (°C) Mean (*n*)	Depth [2] (km) Mean	Tm (°C) min/max	Tm (°C) Mean (*n*)	Salinity [3] (wt.% eq) NaCl	Salinity [3] (wt.% eq) $CaCl_2$
1	Kumsai C_2b	818	1 2	52.3/61.5 102/111	56.9 (2) 107.6 (3)	1.2 2.9	−32.8/−10 −38/−7	−21.4 (2) −22.5 (2)		24.0 24.4
2	Kumsai D_2g–D_3fr	813	1 2 3 4	68 85/146 164 185	68 (1) 113 (1) 164 (1) 185 (1)	1.6 3.1 4.8 5.5	- −23/−6 - −2	- −14.24 (9) - −2 (1)	18 3.4	19.8 3.8
3	Kumsai D_2–D_3	811	1 2 3 4	56.5/78 98.5/146 155/165 190	66.08 (13) 115 (9) 160 (2) 190 (1)	1.5 3.2 4.7 5.7	−20/−4 −8/−4 −2 −10	−13 (13) −5.57 (7) −2 (1) −10 (1)	16.9 8.6 3.4 13.9	18.8 9.9 3.8 15.8
4	Alexandrov Fold P_1	B16	2 4	87/106 180/238	98 (4) 220 (9)	2.5 6.7	−0.7/−0.4 −3.5/−0.7	−0.5 (4) −1.38 (9)	0.9 2.4	0.8 2.6
5	Koktobe P_1s	795	1 2	74 92.5	74 (1) 92.5 (1)	1.8 2.4	−6 -	−6 (1) -		
6	Karnak P_1as	832	2	92.5	92.5 (1)	2.4	0	0 (1)	0	0
7	Dombar area C_1v-s	B19	2	97/139	100 (17)	2.5	−7.7/−3	−5.6 (18)	8.7	10.0

Table 2. *Cont.*

No.	Location Age	Sample No.	Population	Th (°C)		Depth [2] (km)	Tm (°C)		Salinity [3] (wt.% eq)	
				min/max	Mean (*n*)	Mean	min/max	Mean (*n*)	NaCl	$CaCl_2$
8	Shandy Fm $D_{1–2}$	E23	3	153/166	159 (6)	4.6	−4/−2	−3.08 (6)	5.1	5.8
9	Sakmara Fm $S_{3–4}$	E26	1	54/70	62 (6)	1.3	−4.3/−0.2	−1.7 (6)	2.9	3.2
			2	91/130	104 (12)	2.7	−5.3/−4.7	−4.8 (10)	7.6	8.7
			4	183/219	204 (12)	6.2	−4.3/−0.6	−1.04 (13)	1.8	1.9
10	Chanchar Fm D_2	K15	2	116/133	125 (8)	3.5	−3.3/−1.1	−2.2 (8)	3.7	4.1
			3	157/168	162 (5)	5.2	−3.3/−0.9	−2.1 (5)	3.6	4.0
			4	188/229	211 (5)	7.0	−4/−1.2	−2.4 (5)	4.	4.5
			5	268/284	277 (7)	8.8	−4/−1.1	−2.8 (7)	4.7	5.3

[1] Minimum, maximum, and modal values are shown; *n* = number of measurements (in parentheses). [2] Apparent equivalent depth calculated assuming a conductive geothermal gradient of 30 °C/km. Mean annual surface temperatures ranged from ~15 °C during Early Devonian [43] to ~30 °C [44], with cooling to ~5 °C during the Middle Devonian. A representative mean surface temperature of 20 °C was therefore adopted for depth estimates. [3] Salinities exceeding the eutectic (−21.1 °C; 23.3 wt.% NaCl equation) indicate the presence of $CaCl_2$ (antarcticite); in such a case, salinity should be expressed as wt.% $CaCl_2$ equivalent. Salinities were calculated from Th using the equations of Potter et al. [46,47], Bodnar et al. [46], and Steele-MacInnis et al. [48]. Abbreviations: Tm—final ice-melting temperature; Th—homogenization temperature. Multiple Th–Tm populations within individual samples indicate several generations of fluid inclusions, likely associated with successive burial, tectonic, and hydrothermal events. Five fluid inclusion populations are recognized: (1) low-temperature (50–78 °C), (2) burial-related (85–146 °C), (3) intermediate (155–176 °C), (4) elevated (183–242 °C), and (5) high-temperature (275–284 °C).

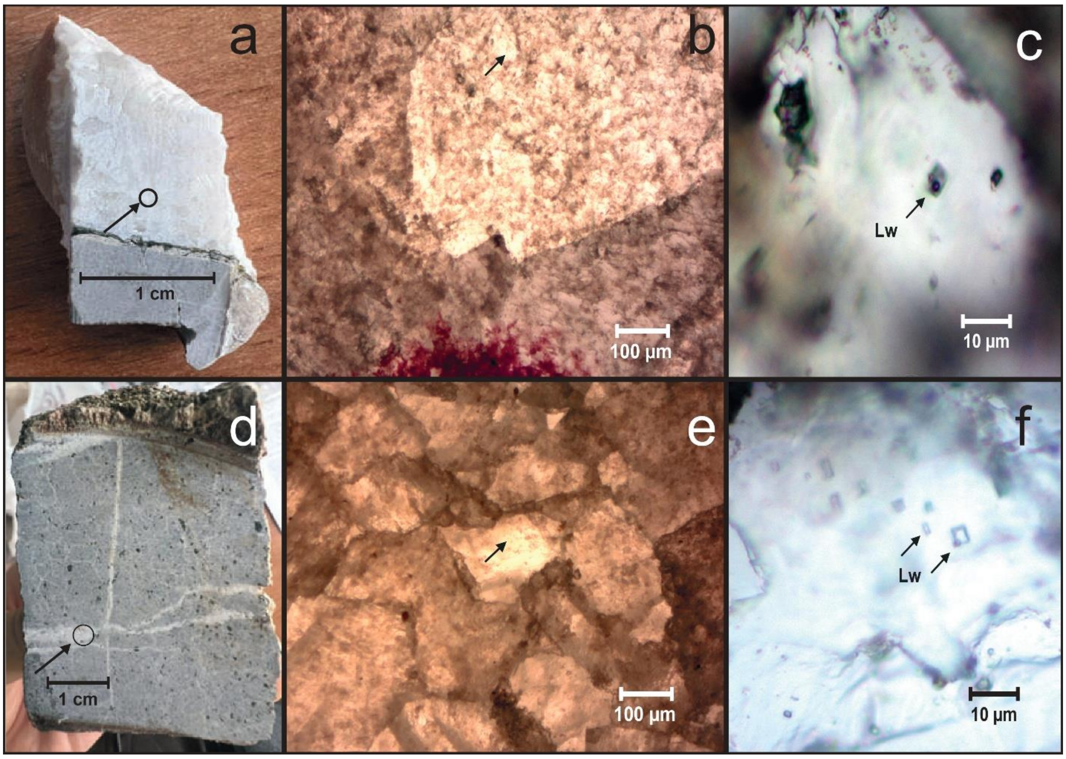

Figure 4. Petrographic occurrence and fluid inclusion assemblages in calcite veins and recrystallized microfractures from samples E-26 (Sakmar Formation, Upper Silurian, $S_{3–4}$) (**a**–**c**) and E-23 (Shandy Formation, Lower–Middle Devonian, $D_{1–2}$) (**d**–**f**). (**a**) Macrophoto of sample E-26 showing a calcite-filled vein/fracture; (**b**) photomicrograph of the calcite-bearing zone (10×); (**c**) two-phase aqueous fluid inclusions hosted in calcite (100×); (**d**) macrophoto of sample E-23 showing a network of calcite veins; (**e**) photomicrograph of a calcite veinlet and adjacent recrystallized calcite zone (10×); (**f**) two-phase aqueous fluid inclusions hosted in calcite (100×).

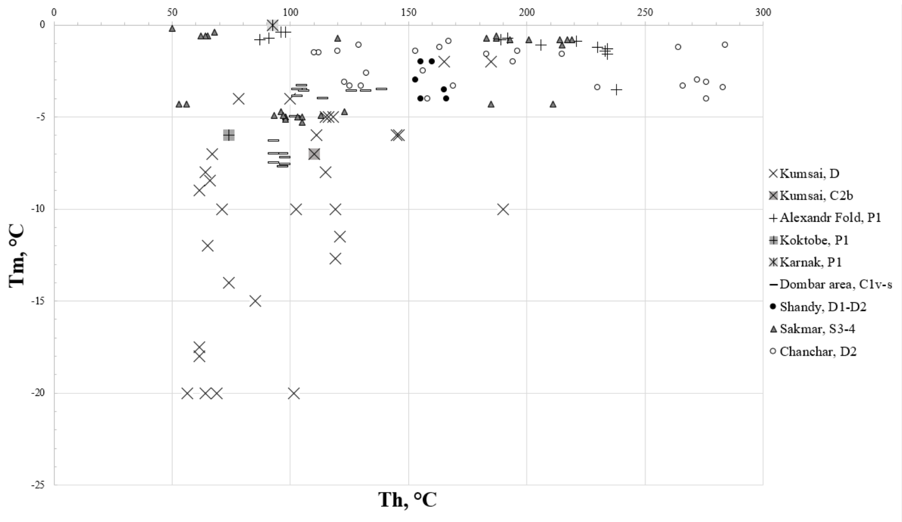

Figure 5. Relationship between homogenization temperature (Th) and final ice-melting temperature (Tm) of aqueous fluid inclusions hosted in calcite from Paleozoic limestones of the Pre-Uralian Foredeep and the Sakmara accretionary zone (Mugodzhar). Distinct low-, burial-related, intermediate-, elevated, and high-temperature populations are identified, reflecting different stages of fluid entrapment and thermal evolution, including background burial heating and superimposed transient hydrothermal pulses. Symbol colors denote different localities and stratigraphic units.

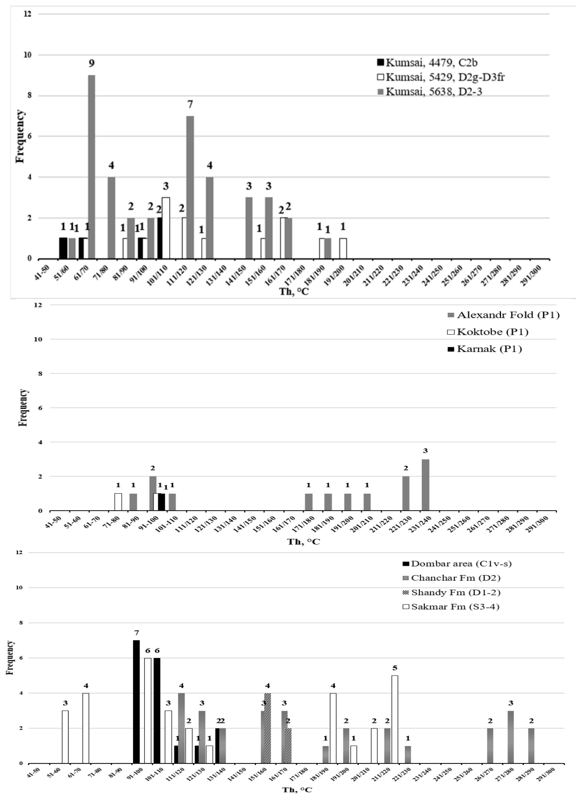

(a) (b) (c)

Figure 6. Frequency distribution (histogram) of homogenization temperatures (Th) of aqueous fluid inclusions from: (**a**) the Kumsai well (eastern Pre-Caspian Basin), (**b**) the Alexandrov Fold, the Koktobe and Karnak wells (Pre-Uralian Foredeep), (**c**) the Dombar area, and the Chanchar and Sakmara formations (Sakmara zone). The dominant burial-related population (Th ≈ 87–146 °C) reflects regional burial heating, whereas low-temperature populations record early diagenetic and/or late-stage fluid circulation. Elevated and high-temperature populations indicate transient, structurally controlled hydrothermal pulses associated with fault- and fracture-guided fluid flow.

4. Results

4.1. Fluid Inclusion Types

The studied inclusions are predominantly two-phase aqueous liquid–vapor (Lw) inclusions occurring in calcite that fills microfractures and small veins. They are interpreted as primary or pseudosecondary inclusions associated with fracture-controlled calcite precipitation. In several samples, multiple inclusion assemblages occur within a single calcite generation, indicating multiple episodes of fluid entrapment (Figure 4).

Fluid inclusions occur predominantly in calcite filling healed microfractures and small veins, which constitute the principal host phases in the studied samples. Additional inclusions were identified in fracture-related calcite within two litharenite samples from the Karnak and Koktobe wells.

Geological and tectonic constraints indicate moderate burial depths for the Paleozoic sedimentary successions (generally on the order of ~2–4 km), corresponding to low to moderate temperatures under conductive geothermal gradients. However, fluid inclusions in carbonate veins and fractures locally yield homogenization temperatures significantly higher than those expected from burial heating alone, suggesting transient thermal anomalies and/or fault-controlled advective heat transfer.

4.2. Homogenization Temperatures (Th)

Homogenization temperatures (Th) range from ~50 to 284 °C and define several distinct populations (Figures 5 and 6):

- Low-temperature: 50–78 °C;
- Intermediate: 87–146 °C, buried related;
- Moderately high: 155–166 °C (Devonian limestones, Shandy Formation):
- High: >180 °C, locally reaching ~275–284 °C occurring in fracture- and vein-filling calcite.

(**a**) (**b**) (**c**)

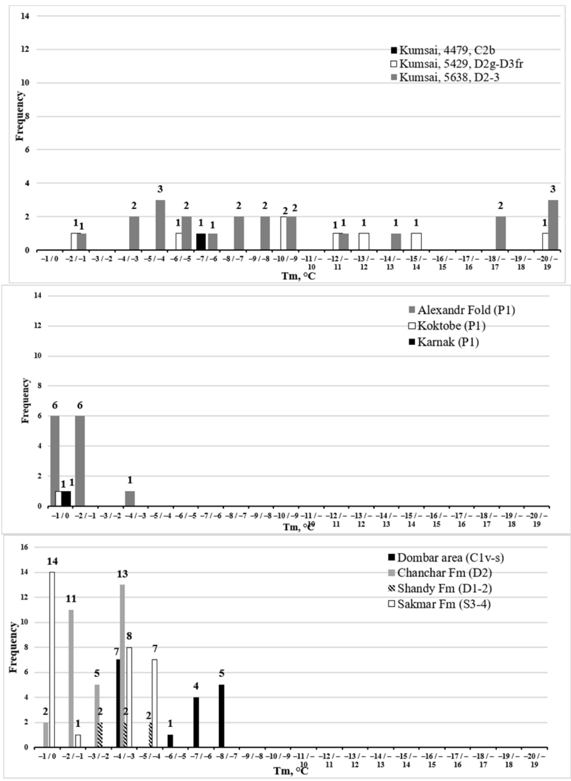

Figure 7. Frequency distribution (histogram) of final ice-melting temperatures (Tm) of aqueous fluid inclusions in sedimentary rock samples from (**a**) the Alexandrov Fold (Pre-Uralian Foredeep),

(**b**) the Dombar area, and (**c**) the Chanchar and Sakmara formations (Sakmara zone). The distributions indicate predominantly low- to moderate-salinity fluids, with only minor variability among localities, consistent with mixed basinal and formation-water compositions. Within individual samples, the burial-related and intermediate-temperature populations generally exhibit relatively narrow Tm ranges, suggesting chemically similar fluid sources during individual fluid-flow events.

4.3. Ice-Melting Temperatures (Tm) and Salinity

Final ice-melting temperatures (Tm) range from near 0 °C to ≈ -8 °C in most samples, indicating low- to moderately saline aqueous fluids (Figure 7). More negative Tm values occur in several samples from the eastern margin of the Pre-Caspian Basin, reaching ≈ -20 °C and indicating higher salinities.

Salinities exceeding the metastable eutectic of the H_2O-NaCl system (-21.1 °C; 23.3 wt.% NaCl equation) [49–53] indicate the presence of $CaCl_2$ (antarcticite) and are therefore expressed as wt.% $CaCl_2$, equivalents using equations for the H_2O-NaCl-$CaCl_2$ system [45–48]. Freezing-point depressions correspond to $\approx 11.68 \pm 0.03$ wt.% NaCl equation for Tm ≈ -8 °C and $\approx 23.4 \pm 0.1$ wt.% $CaCl_2$ equation for Tm ≈ -20 °C [45,46].

4.4. Pressure–Temperature Constraints

Isochore calculations based on equations of state for aqueous H_2O-NaCl inclusions indicate trapping depths of ~1.8–2.5 km for inclusions with homogenization temperatures of 50–78 °C, assuming near-hydrostatic pressure typical of carbonate-hosted systems.

Inclusions with Th $\approx$ 87–146 °C yield the apparent trapping temperatures consistent with independently inferred burial depths of approximately 2–4.5 km under low to moderate geothermal gradients.

In contrast, inclusions with Th > 180 °C record temperatures significantly higher than those expected from conductive burial heating at the reconstructed depths. These inclusions are therefore interpreted as evidence of transient, fracture- or fault-controlled hydrothermal pulses rather than regional burial conditions.

The occurrence of fluid inclusions in fracture-filling calcite, together with the wide range of homogenization temperatures, indicates that fluid circulation was strongly controlled by fracture and fault networks associated with the tectonic evolution of the accretionary complex.

5. Discussion

5.1. Overview: A Polyphase, Predominantly Fracture-Controlled Record

A rigorous P–T–t reconstruction is limited by the absence of direct chronological constraints on the fracture- and vein-filling calcites studied here. Fluid inclusions occur mainly in calcite-filled microfractures and, less commonly, in small veins. Because inclusion-bearing veins are scarce and systematic structural data for different fracture generations are lacking at many localities, the relative chronology of fracture systems cannot be established with confidence. The identified fluid-inclusion populations should therefore be interpreted as thermal-fluid regimes constrained by microthermometry and regional geology rather than as precisely dated events.

The Th–Tm data record fluid entrapment during episodes of calcite precipitation and fracture sealing. Accordingly, they are used to evaluate fluid-related thermal events and their compatibility with independently constrained burial and maturity data, rather than to reconstruct the complete thermal history of the host rocks.

In the Devonian and Carboniferous units, fracture development and reactivation were likely associated with Late Carboniferous–Early Permian collisional deformation during the final stages of Uralian convergence. In contrast, the Silurian Sakmara Formation records a more complex history involving accretionary processes followed by collisional overprinting, making the relationships between fracture generations less certain. The proposed evolution is therefore interpreted as a relative progression from burial-related diagenetic fluids to increasingly focused fracture-controlled circulation and localized hydrothermal pulses, rather than as a fully constrained chronological P–T–t path.

The fluid-inclusion dataset documents a polyphase fluid evolution across structurally distinct domains of the Southern Urals–western Kazakhstan region. Most inclusions occur in calcite-sealed microfractures and veins, indicating that fluid trapping postdated sedimentation and was mainly associated with fracture formation and sealing during Late Paleozoic tectonic reorganization. Consequently, the Th–Tm data mainly reflect the evolution of fracture-controlled permeability and episodic fluid circulation, rather than a simple burial-driven thermal history.

The geological cross-section (Figure 3) indicates that the Silurian–Carboniferous units hosting fluid inclusions were buried to relatively modest depths (~2–4 km) within the frontal thrust zone, whereas significantly greater burial occurred in the adjacent Pre-Uralian Foredeep. Accordingly, the elevated homogenization temperatures are best explained by transient thermal anomalies related to fault-controlled fluid flow and advective heat transfer rather than by conductive burial heating alone. This interpretation is supported by the structural control on fluid pathways and the absence of evidence for regionally pervasive high-temperature burial conditions.

5.2. Burial Temperatures Versus Fluid Inclusion Record

The dominant fluid-inclusion population (Th = 87–146 °C) broadly overlaps the temperature expected from burial heating, indicating that part of the fluid record reflects burial-related thermal evolution. However, several observations suggest that the thermal history cannot be explained solely by conductive heating: (i) the widespread occurrence of low-temperature inclusions (50–78 °C) in the Pre-Caspian Basin, including in units inferred to have experienced deeper burial; (ii) the relative small proportion of inclusions recording temperatures above ~140 °C; and (iii) the coexistence of low- and intermediate-temperature populations within individual samples.

Interpretation of Th as a trapping temperature requires assumptions regarding geothermal gradients because independent temperature constraints are unavailable. Geological and stratigraphic data indicate present-day burial depths of ~2–4.5 km for the studied Paleozoic successions, corresponding to temperatures of roughly ~50–135 °C under typical continental geothermal gradients (25–30 °C/km), with slightly higher values possible depending on heat flow and lithology [51–54] (Figure 8). These estimates are consistent with independently inferred burial depths of ~2.0–2.5 km in the Alexandrov Fold and ~2.2–4.0 km in the Sakmara zone.

Potential biases must also be considered. Although post-entrapment re-equilibration or stretching could increase apparent Th values, the scarcity of high-temperature inclusions, their restriction to specific structural settings, and the absence of petrographic evidence for widespread re-equilibration argue against a dominant effect. Conversely, the preservation of low-temperature inclusions indicates that large-scale thermal resetting did not occur.

Low-temperature inclusions do not necessarily imply survival through a later regional thermal overprint. Instead, the different Th populations are interpreted as products of distinct trapping events within separate calcite-filled microfractures and veinlets. Low-temperature inclusions (Th = 50–78 °C) occur mainly along the eastern Pre-Caspian margin and in the Pre-Uralian Foredeep, but are also present in the oldest Sakmara Formation sample (E26), where they may record either pre-collisional fluid circulation or later fluid flow during cooling and exhumation.

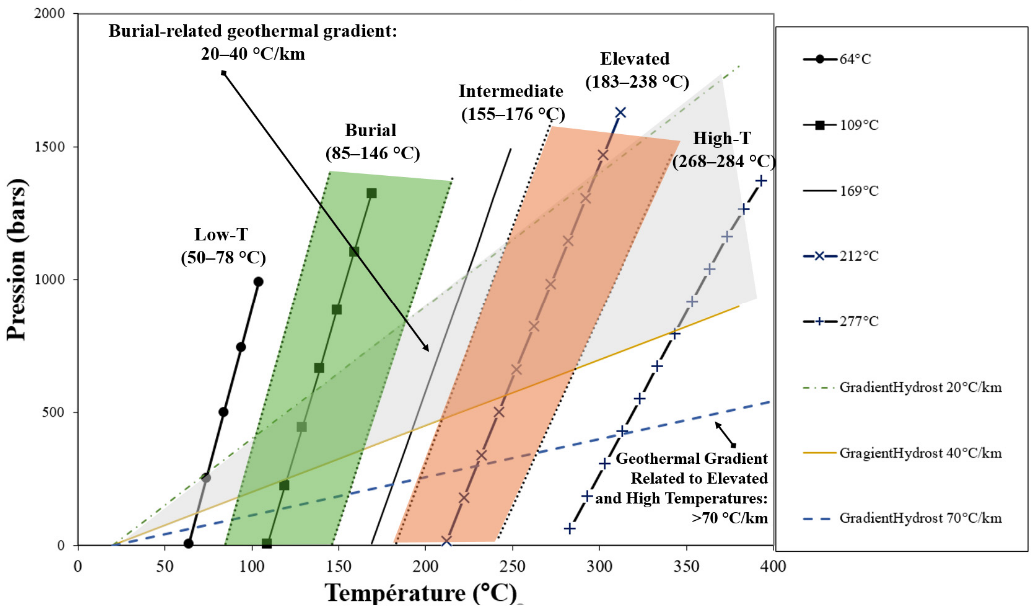

Figure 8. Pressure–temperature (P–T) diagram showing isochores constructed from mean homogenization temperatures of the five fluid inclusion populations: (1) low-temperature (50–78 °C; mean 62 °C), (2) burial-related (85–146 °C; mean 108 °C), (3) intermediate (155–176 °C; mean 169 °C), (4) elevated (183–238 °C; mean 211 °C), and (5) high-temperature (269–284 °C; mean 282 °C). The diagram illustrates the relationship between fluid-inclusion trapping conditions, burial depth, and geothermal gradients, allowing burial-related thermal regimes to be distinguished from localized hydrothermal overprints. The low-temperature and burial-related populations are consistent with trapping under moderate burial conditions, whereas the elevated and high-temperature populations require transient, fault-controlled hydrothermal fluid circulation and advective heat transfer beyond that expected from conductive burial heating alone.

Higher Th values are concentrated in structurally disturbed zones, including the Sakmara Formation, the Alexandrov Fold, and the Chanchar Formation. The highest Th population (276–284 °C), restricted to the Chanchar Formation, most likely records a localized hydrothermal event associated with the Chanchar volcanic complex. Thus, the coexistence of different Th populations within individual samples reflects multiple episodes of fluid entrapment rather than synchronous trapping or regional thermal resetting.

5.3. Low-Temperature Inclusions and Early-to Late-Stage Fluid Circulation

Low-temperature fluid inclusions (Th = 50–78 °C) indicate trapping at relatively shallow depths (~1.8–2.7 km), likely under near-hydrostatic pressure conditions. These inclusions may record either early burial diagenesis prior to maximum subsidence or late-stage fluid infiltration during uplift and exhumation.

Their occurrence alongside higher-temperature populations within the same carbonate successions indicates a multistage fluid history rather than a simple burial-heating trend. As such, they define the lower limit of the system and provide evidence for fluid circulation under relatively mild thermal conditions.

Although a sampling bias toward late-stage vein systems cannot be entirely excluded, the consistent occurrence of multiple fluid inclusion populations within individual samples and across structurally distinct domains supports a genuine multistage fluid evolution rather than a sampling artifact.

5.4. Evidence for a Suppressed Geothermal Gradient

Comparison of fluid-inclusion temperatures with independently constrained burial depths indicates a thermal regime cooler than that expected under typical continental geothermal gradients. Although uncommon, such suppressed geothermal gradients have been documented in specific geodynamic settings.

A well-known example is forearc regions of subduction zones, where geothermal gradients are reduced by the presence of relatively cold subducting lithosphere beneath the overriding plate. Thermal models (e.g., Dumitru, 1991 [55]) predict reduced heat flow and depressed geothermal gradients, consistent with low-temperature, high-pressure metamorphic assemblages such as blueschists [56,57]. The Uralian region is also characterized by relatively low heat-flow densities, attributed in part to limited radiogenic heat production within the crust of the Tagil-Magnitogorsk Zone [58–60].

Although the study area is not an active forearc, the Sakmara accretionary zone represents an ancient accretionary–collisional system that may have inherited a relatively low thermal regime during subduction and early collision. Incorporation of cold material into the accretionary wedge may have contributed to long-lived thermal anomalies.

Low geothermal gradients are also reported in cratonic and platform settings, where reduced lithospheric heat flow persists over long timescales; in rapidly subsiding basins, where sedimentation outpaces thermal equilibration; and in systems affected by large-scale fluid circulation, where advective transport of relatively cool fluids lowers the effective geothermal gradient [58,59].

At the eastern margin of the Pre-Caspian Basin, proximity to the East European Craton likely exerted a first-order control. Cratonic domains are typically characterized by low surface heat flow and reduced geothermal gradients [59], which may explain the relatively low fluid inclusion temperatures despite moderate burial depths.

The fault- and fracture-dominated structural framework likely further enhanced fluid circulation and thermal redistribution. Although advective heat transport can generate localized heating, it can also promote cooling when fluids originate from shallower or cooler reservoirs.

Overall, the data indicate a predominantly low thermal regime resulting from the combined effects of inherited subduction-accretion processes, cratonic thermal influence, and fluid-mediated heat redistribution. Alternative explanations, such as inclusion re-equilibration or sampling bias, cannot be entirely excluded, but they do not adequately explain the consistency of the temperature distributions and their structural relationships. These results show that suppressed geothermal gradients, although relatively uncommon, can develop in complex tectonic settings and persist through subsequent stages of basin evolution.

5.5. Implications for Hydrocarbon Generation

The reconstructed thermal conditions have important implications for hydrocarbon generation. In sedimentary basins, organic matter maturation depends on both temperature and heating duration, with oil generation typically occurring between ~60 and 120 °C and gas generation requiring higher temperatures.

Although some fluid-inclusion temperatures fall within the oil window, several observations suggest limited effective maturation: (i) most temperatures cluster near the lower boundary of the oil window; (ii) the duration of heating remains unconstrained but was likely limited in a tectonically active setting; and (iii) no pervasive high-temperature signal is observed. Together, these observations indicate that peak maturation conditions were not widely attained.

Consequently, in situ hydrocarbon generation was likely limited and spatially restricted. Even where temperatures approached the oil-window conditions, they were probably not sustained long enough to generate significant hydrocarbon volumes.

5.6. Hydrocarbon Origin: Migration Versus Local Generation

Given the limited evidence for sufficient thermal maturity, hydrocarbons present in the region were likely not generated within the studied formations. A more plausible interpretation is that they originated in deeper, more thermally mature parts of the basin or in adjacent domains and subsequently migrated into the studied units.

In this context, the structural framework played a critical role. Major fault systems, including the Main Uralian Fault and associated thrusts, provided efficient pathways for both vertical and lateral migration. The same fracture networks that host fluid inclusions likely served as conduits for hydrocarbon transport.

This interpretation is consistent with petroleum systems in many foreland basins, where hydrocarbons generated in deeper depocenters migrate into structurally elevated or less mature reservoirs.

5.7. Transient Hydrothermal Events and Their Limited Thermal Significance

High-temperature fluid inclusions (Th > 180 °C, locally up to ~280 °C) represent a distinct component of the thermal record. These temperatures are inconsistent with conductive heating at the reconstructed burial depths (2–4 km) and would require unrealistically high geothermal gradients under steady-state conditions.

These inclusions are best interpreted as recording short-lived hydrothermal events associated with fault-controlled fluid flow, transient permeability enhancement, and localized advective heat transport, as observed in rift environments [51–54]. Such hydrothermal pulses are well documented in orogenic and foreland settings, where tectonic activity promotes focused fluid circulation, although their spatial and temporal extent is generally limited ([55,56]). In the present case, several observations indicate that these events did not significantly modify the regional thermal regime: high-temperature inclusions are uncommon, restricted to specific structural settings, and coexist with much lower-temperature populations.

Thus, although hydrothermal events locally generated elevated temperatures, they represent superimposed thermal anomalies rather than the dominant thermal regime.

Independent paleothermal and maturity constraints for the Mugodzhary segment of the Southern Urals remain limited and are not always directly comparable with the present fluid-inclusion (FI) dataset. Previous studies from the eastern Pre-Caspian Basin and the Pre-Uralian Foredeep reported Rock–Eval T_{max}, vitrinite reflectance, molecular maturity indicators, and 2D basin-modeling results indicating that the onset of the oil window generally occurs at depths of ~3.2–4.0 km, with maturity increasing eastward toward the Pre-Uralian Basin (Rv = 0,55%, Tmax = 430 °C) and the Uralian suture zone (Rv = 1,1%, Tmax = 462 °C) [24,57–59]. The most relevant comparison is provided by vitrinite reflectance and Rock–Eval data from the Izembet well, located in the frontal Sakmara thrust zone (Figures 1B and 3) [24].

Additional constraints are provided by low-temperature thermochronology and present-day heat-flow studies. $^{40}Ar/^{39}Ar$ data from the Maksyutov metamorphic complex record a Devonian to Late Carboniferous–Early Permian tectono-thermal history involving high-pressure metamorphism, cooling, and exhumation during the Uralian orogeny [58]. Apatite fission-track data further indicate cooling and exhumation of the Maksyutov Complex through temperatures of approximately 110 °C during the Early Permian (~300 ± 25 Ma) [58]. Present-day heat-flow measurements from the Ural fold belt indicate a generally low conductive thermal background [59–63]. However, these datasets do not directly constrain Paleozoic heat flow during fluid-inclusion entrapment and therefore provide only a regional tectono-thermal context rather than quantitative constraints on the thermal conditions recorded by the studied fluid inclusions.

To further evaluate the elevated and high-temperature FI populations, our results were compared with regional studies from the Southern Urals that independently support the occurrence of localized high-temperature hydrothermal pulses. Rakhimov et al. (2023) [64] reported gold-bearing quartz veins from the Khudolaz area, where gold precipitated at 230–330 °C from low- to moderate-salinity H_2O–CO_2–CH_4 fluids of predominantly magmatogenic origin associated with Late Carboniferous mafic–ultramafic to gabbro–diorite intrusions. Korekina and Savichev (2023) [65] documented hydrothermal to hydrothermal–metamorphic fluid inclusions (230–440 °C) in barren quartz veins from the Middle and Southern Urals, demonstrating that high-temperature fluid circulation also occurred in non-mineralized systems. Sharipova et al. (2017) [66] reported primary fluid inclusions in quartz veins from the Avzyan gold district with Th = 228–382 °C, interpreted as magmatogenic to post-magmatic fluids related to deep fluid migration during regional tectono-thermal activity.

Although these quartz-vein systems are not direct analogues of the carbonate-hosted inclusions studied here, they demonstrate that short-lived high-temperature fluid pulses were regionally plausible within the Southern Ural orogenic domain. Consequently, the elevated Th populations identified in this study are best interpreted as localized, fracture-controlled hydrothermal anomalies rather than evidence of pervasive regional thermal resetting.

5.8. Progressive Localization of Permeability: A Continuum Rather than Discrete "Events"

Across the dataset, the Th populations show partial overlap and gradational transitions, indicating a continuum of evolving fluid–rock interaction rather than a series of discrete thermal events. A useful framework is progressive permeability localization, whereby early fluid flow occurs diffusely through the rock matrix and fine microfractures, while continued deformation progressively focuses flow into interconnected microfracture networks and larger fractures or veins.

Within this framework, the intermediate temperature population (Th ≈ 150–170 °C) represents a transitional regime in which both diffuse and fracture-controlled flow contributed to fluid circulation, producing overlapping Th–Tm fields and intermediate thermal signatures.

5.9. Pressure–Temperature Constraints and Trapping Depths

The integrated results combine homogenization-temperature populations, isochore reconstructions, and reference geothermal gradients, allowing burial-related thermal conditions to be distinguished from structurally controlled advective overprints.

Together, these results provide a concise summary of estimated trapping depths, apparent thermal gradients, and the probable timing of fluid entrapment conditions, linking the microthermometric dataset to the burial, deformation, and hydrothermal evolution of the Sakmara accretionary zone and the adjacent Pre-Uralian Foredeep.

The estimated trapping depths provide first-order constraints on fluid inclusion entrapment. Low- to intermediate-temperature populations are broadly consistent with burial-related conditions, whereas the highest-temperature populations require localized advective heating at relatively modest depths.

Table 3 summarizes a conceptual tectono-thermal model relating the principal fluid-inclusion temperature populations to the tectono-stratigraphic evolution of the eastern Pre-Caspian Basin, the Pre-Uralian Foredeep, and the Sakmara thrust/accretionary zone. Because direct dating of vein minerals is unavailable, the framework is interpreted as a relative sequence of thermal-fluid regimes rather than a strictly chronological sequence of fluid events.

Table 3. Conceptual tectono-thermal framework for interpreting fluid-inclusion populations in the eastern Pre-Caspian Basin, the Pre-Uralian Foredeep, and the Sakmara thrust/accretionary zone.

Geodynamic Stage	Age	Main Domain	Formations	FI Populations	Interpreted Fluid Regime
Oceanic/rift- to early marginal-basin	Ordovician–Silurian	Sakmara zone	Sakmara Fm	Low-T to burial-related	Early background thermal regime, later partly overprinted by burial and accretional/collisional processes
Subduction–accretion and early collision	Devonian–Tournaisian	Sakmara accretionary zone	Sakmara, Shandy, Chanchar	Burial-related, intermediate, elevated, locally high-T	Fault- and fracture-controlled advective/hydrothermal pulses
Collision and foreland loading	Late Carboniferous–Permian	Pre-Uralian Foredeep, Sakmara thrust front, eastern Pre-Caspian Basin	Dombar, Alexandrov, Sakmara, Kumsai	Burial-related, to locally high-T	Burial fluids combined with structurally focused flow during thrusting
Post-collisional uplift/reactivation	Permian and younger	Thrust front, foredeep margin, eastern Pre-Caspian Basin	Calcite-filled fractures and veins in outcrops and wells	Low-T and mixed	Low-T meteoric/formational circulation, local reactivation, and late fracture-controlled flow

This conceptual framework indicates that the studied inclusions do not represent a fully dated succession of fluid events but rather a polyphase, predominantly fracture-controlled fluid system. Burial-related fluids were progressively overprinted by localized advective and hydrothermal pulses, allowing the coexistence of preserved low-temperature signatures and rare high-temperature inclusions. The latter are therefore interpreted as transient, structurally focused thermal anomalies rather than evidence of a regionally pervasive high-temperature burial regime.

6. Conclusions

1. The studied fluid inclusions record a polyphase, predominantly fracture-controlled fluid system comprising several thermal populations distinguished by homogenization temperature, salinity, and host microstructural setting. Because direct dating of vein minerals and systematic structural constraints on distinct fracture generations are unavailable, the proposed *early-*, *intermediate-*, and *high*-temperature stages should be interpreted as a relative sequence of thermal-fluid regimes within the regional tectonic framework rather than as a fully resolved chronological evolution.
2. Fluid inclusion microthermometry reveals a complex, multistage thermal history. The dominant population (Th $\approx$ 87–146 °C) records burial-related fluids at depths of approximately 2–4.5 km. Higher-temperature inclusions (Th > 180 °C) indicate short-lived fault-controlled hydrothermal pulses and advective heat transfer, whereas lower-temperature inclusions (Th $\approx$ 50–78 °C) reflect early burial diagenesis and/or late-stage fluid circulation during uplift and exhumation.
3. The thermal evolution of the Pre-Uralian Foredeep and Sakmara accretionary zone reflects the combined effects of burial heating and episodic hydrothermal circulation. The available fluid-inclusion, structural, and maturity data suggest that hydrocarbons were likely generated in deeper, more thermally mature source intervals and subsequently migrated into the studied formations along fault-controlled pathways.

4. This study highlights the value of integrating fluid-inclusion microthermometry with structural and burial-history analyses to reconstruct basin-scale thermal and fluid-flow evolution. The resulting conceptual model is applicable to other collisional belts and foreland basins where transient hydrothermal circulation along major tectonic structures influences diagenesis, thermal evolution, and petroleum-system development.
5. The principal limitation of this study is the absence of direct geochronological constraints on vein formation and fluid entrapment. Additional uncertainty arises from the limited number of studied localities and the incomplete characterization of fracture generations and paleostress histories. Consequently, the proposed thermal-fluid evolution should be regarded as a first-order conceptual framework rather than a fully constrained P–T–t reconstruction.
6. Future research should integrate fluid-inclusion studies with vein-mineral geochronology (e.g., U–Pb and Ar–Ar methods), low-temperature thermochronology, stable-isotope geochemistry, basin modeling, and detailed structural analysis. Such multidisciplinary approaches would better constrain the timing of fluid-flow events, quantify the relative contributions of conductive and advective heat transfer, and refine petroleum-system models for the Uralian foreland system and analogous basins worldwide.

Overall, the results show that transient, fault-controlled hydrothermal circulation can significantly modify the thermal evolution of collisional and foreland basins beyond the effects of conductive burial alone. The fluid-inclusion record reveals a polyphase fluid history dominated by burial-related fluids and locally overprinted by short-lived hydrothermal pulses. Similar processes documented in foreland basins worldwide suggest that localized hydrothermal events may represent an important, yet commonly underappreciated, control on basin evolution, reservoir diagenesis, and hydrocarbon migration.

Author Contributions: Conceptualization, T.Y. and M.C.; methodology, T.Y. and M.C.; software, I.K.; validation, T.Y., A.A., I.K. and J.-J.R.; formal analysis, T.Y. and J.-J.R.; investigation, T.Y. and I.K.; resources, T.Y.; data curation, T.Y., A.A. and L.N.; writing—original draft preparation, T.Y., I.K. and L.N.; writing—review and editing, T.Y., J.-J.R. and M.C., visualization, T.Y., J.-J.R. and M.C.; supervision, T.Y. and M.C.; project administration, T.Y.; funding acquisition, T.Y. All authors have read and agreed to the published version of the manuscript.

Funding: This research was funded by the Committee of Science of the Ministry of Science and Higher Education of the Republic of Kazakhstan (Grant Bo. AP23489821), entitled "Geological-geochemical, microthermometric studies of oil-generating formations and new resources' forecast of south-eastern side of Precaspian syneclise and Ural Mugodzhar (2024–2026)".

Data Availability Statement: The data supporting this study are available from the corresponding author upon reasonable request.

Acknowledgments: The authors thank the administration of K.I. Satpayev Kazakh National Technical Research University for providing organizational and institutional support.

Conflicts of Interest: The authors declare no conflicts of interest. A ChatGPT4.5-based language tool was used for English editing. All scientific content, interpretations, and conclusions are the responsibility of the authors.

Abbreviations

The following abbreviations are used in this manuscript:

FI	Fluid inclusion
Fm	Formation

https://doi.org/10.3390/geosciences16070260

Tm	Final ice-melting temperature
Th	Homogenization temperature
P-T	Pressure–temperature
wt.%	Weight per cent

References

1. Moretto, V.; Berio, L.R.; Dallai, L.; Viola, G.; Balsamo, F.; Pizzati, M.; Grathoff, G.; Warr, L.N.; Xie, R.; Aldega, L. Unmixing fluid histories in polymineralic fault rocks using isotopic evolution and the PolyFrac tool: A case study from Lemnos Island, Greece. *Chem. Geol.* **2026**, *708*, 123345. [CrossRef]
2. Spagnolo, G.S.; Bernasconi, S.M.; Aldega, L.; Castorina, F.; Billi, A.; Smeraglia, L.; Agosta, F.; Prosser, G.; Tavani, S.; Carminati, E. Interplay and feedback between tectonic regime, faulting, sealing horizons, and fluid flow in a hydrocarbon-hosting extensional basin: The Val d'Agri Basin case, Southern Italy. *Earth Planet. Sci. Lett.* **2024**, *646*, 118982. [CrossRef]
3. Rauch, C.; Barrie, K.; Collins, S.C.; Hornbach, M.J.; Brokaw, C. Heat flow and thermal conductivity measurements in the northeastern Pennsylvania Appalachian Basin depocenter. *AAPG Bull.* **2018**, *102*, 2155–2170. [CrossRef]
4. Kingston, A.; Ardakani, O.H.; Watt, E.; Samson, I.M. Evidence of Hydrocarbon Generation and Overpressure Development in an Unconventional Reservoir Using Fluid Inclusion and Stable Isotope Analysis From the Early Triassic, Western Canadian Sedimentary Basin. *Front. Earth Sci.* **2022**, *10*, 918898. [CrossRef]
5. Delpomdor, F.; Bonneville, S.; Baert, K.; Préat, A. An introduction to the Precambrian petroleum system in the Sankuru-Mbuji-Mayi-Lomami-Lovoy Basin, South-Central Democratic Republic of Congo. *J. Pet. Geol.* **2017**, *41*, 5–27. [CrossRef]
6. Opera, A.; Alizadeh, B.; Sarafdokht, H.; Janbaz, M.; Fouladvand, R.; Heidarifard, M.H. Burial history reconstruction and thermal maturity modeling for the Middle Cretaceous–Early Miocene Petroleum System, southern Dezful Embayment, SW Iran. *Int. J. Coal Geol.* **2013**, *120*, 1–14. [CrossRef]
7. Barnolas, A.; Larrasoaña, J.C.; Pujalte, V.; Schmitz, B.; Sierro, F.J.; Mata, M.P.; van den Berg, B.C.J.; Pérez-Asensio, J.N.; Salazar, Á.; Salvany, J.M.; et al. Alpine Foreland Basins. In *The Geology of Iberia: A Geodynamic Approach. Regional Geology Reviews*; Quesada, C., Oliveira, J., Eds.; Springer: Cham, Switzerland, 2019. [CrossRef]
8. Mukhtarova, K.Z.; Nasibova, G.J. Geodynamic regime and prospects for oil and gas potential in the South Caspian Basin. *J. Geol. Geogr. Geoecology* **2023**, *32*, 550–559. [CrossRef] [PubMed]
9. Ullah, I.; Jamil, M.; Rahim, H.U.; Khan, I.; Ali, A.; Muzammil, M.; Abbas, W.; Umar, M.; Shah, F.; Usman, M. Impact of Diagenesis on Microbial Carbonate Reservoirs in the Upper Indus Basin, NW Himalayas. *Minerals* **2026**, *16*, 111. [CrossRef]
10. González-Acebrón, L.; Goldstein, R.H.; Mas, R.; Arribas, J. Criteria for recognition of localization and timing of multiple events of hydrothermal alteration in sandstones illustrated by petrographic, fluid inclusion, and isotopic analysis of the Tera Group, Northern Spain. *Int. J. Earth Sci.* **2011**, *100*, 1811–1826. [CrossRef]
11. Bahnan, A.E.; Carpentier, C.; Pironon, J.; Ford, M.; Ducoux, M.; Barré, G.; Mangenot, X.; Gaucher, E.C. Impact of geodynamics on fluid circulation and diagenesis of carbonate reservoirs in a foreland basin: Example of the Upper Lacq reservoir (Aquitaine basin, SW France). *Mar. Pet. Geol.* **2020**, *111*, 676–694. [CrossRef]
12. de Graaf, S.; Nooitgedacht, C.W.; Le Goff, J.; van der Lubbe, J.H.J.L.; Vonhof, H.B.; Reijmer, J.J.G. Fluid-flow evolution in the Albanide fold-thrust belt; insights from hydrogen and oxygen isotope ratios of fluid inclusions. *AAPG Bull.* **2019**, *103*, 2421–2445. [CrossRef]
13. Zhemchuzhnikov, V.; Akhmetzhanov, A.; Ibrashev, K.; Akhmetzhanova, G. The Geotectonic Peculiarities of the North Caspian Permian Salt-Bearing Basins (Kazakhstan). *Geosciences* **2024**, *14*, 23. [CrossRef]
14. Abdulin, A.A.; Avdeev, A.V.; Seitov, N.S. *Tectonics of the Sakmara and Or-Ilek Zones of the Mugodzhar*; Nauka: Alma-Ata, Kazakhstan, 1977; 238p. (In Russian)
15. Abdulin, A.A.; Zaravnyaeva, V.K.; Korinevsky, V.G. New Data on the Stratigraphy of the Greenstone Volcanogenic Zone of the Southern Mugodzhar. In *Problems of Geology and Copper Mineralization of the Mugodzhar*; Nauka: Alma-Ata, Kazakhstan, 1963; pp. 26–39.
16. Peive, A.V.; Ivanov, S.N.; Necheukhin, V.M.; Perfil'ev, A.S.; Puchkov, V.N. *Tectonics of the Urals: Explanatory Note to the Tectonic Map of the Urals at 1:1,000,000 Scale*; Nauka: Moscow, Russia, 1977; 120p. (In Russian)
17. Ruzhentsev, S.V. Geology of the Southern Part of the Sakmara Zone of the Urals. In *Problems of Theoretical and Regional Tectonics*; Nauka: Moscow, Russia, 1971; pp. 25–40. (In Russian)
18. Ruzhentsev, S.V. *Marginal Ophiolitic Allochthons*; Nauka: Moscow, Russia, 1976; 170p. (In Russian)
19. Ivanov, S.N.; Puchkov, V.N.; Ivanov, K.S.; Samarkin, G.I.; Semenov, I.V.; Pumpyansky, A.I.; Dymkin, A.M.; Poltavets, Y.A.; Rusin, A.I.; Krasnobaev, A.A. *Formation of the Earth's Crust of the Urals*; Nauka: Moscow, Russia, 1986; 248p.
20. Montenat, C.; Barrier, P.; Francou, C. Oural = Ural = Urali. In *Documents et Travaux de L'IGAL; Mémoire Hors-Série 1*; Institut Géologique Albert-de-Lapparent: Cergy-Pontoise, France, 1995; 189p.
21. Puchkov, V.N. *Paleo Geodynamics of the Southern and Middle Urals*; Gilem Publishing House: Ufa, Russia, 2000; 146p. (In Russian)

22. Puchkov, V.N. *Geology of the Urals and Cis-Urals: Actual Problems of Stratigraphy, Tectonics, Geodynamics and Metallogeny*; Design-PoligraphService: Ufa, Russia, 2010; 280p. (In Russian)
23. Yurish, V.V.; Ulukpanov, K.T. *Geodynamics of the Paleozoic of the Kazakh Urals*; Aktobe Regional University Press: Aktobe, Kazakhstan, 2020. (In Russian)
24. Yensepbayev, T.A.; Izart, A.; Joltaev, G.; Hautevelle, Y.; Suarez-Ruiz, I. Geochemical characterization of source rocks and oils from the eastern part of the Precaspian basin and Pre-Uralian basin (Kazakhstan): Paleoenvironmental and paleothermal interpretation. *Org. Geochem.* **2010**, *41*, 242–262. [CrossRef]
25. Khvorova, I.V.; Voznesenskaya, T.A.; Zolotarev, B.P.; Il'inskaya, M.N.; Ruzhentsev, S.V. *Formations of the Sakmara Allochthon*; Nauka: Moscow, Russia, 1978; 232p. Available online: https://www.geokniga.org/labels/55166 (accessed on 22 June 2026). (In Russian)
26. Leonenok, N.I. Silurian Deposits of the Kos-Istek Area, Northern Mugodzhar. *Tr. Lab. Geol. Uglya* **1955**, *3*, 116–225. (In Russian)
27. Varganov, V.G.; Antsygin, N.Y.; Nasedkina, V.A.; Militsina, V.S.; Shurygina, M.V. *Stratigraphy and Fauna of the Ordovician of the Middle Urals*; Nedra: Moscow, Russia, 1973; 227p. Available online: https://www.dissercat.com/content/stratigrafiya-i-khitinozoi-ordovika-zilairskogo-sinklinoriya-yuzhnogo-urala (accessed on 22 June 2026). (In Russian)
28. Nasedkina, V.A. Ordovician Conodonts of the Western Slope of the Urals. In *New Miospores, Foraminifers, Ostracods and Conodonts of the Paleozoic and Mesozoic of the Urals*; Malakhova, N.P., Chuvashov, B.I., Eds.; Ural Scientific Center, USSR Academy of Sciences: Sverdlovsk, USSR, 1975; pp. 110–136. (In Russian)
29. Korinevsky, V.G. Volcanogenic Rocks of the Lower Silurian of the Sakmara Zone of the Mugodzhar. In *Problems of Petrology of Volcanic Rocks of the Urals*; Ural Scientific Center, USSR Academy of Sciences: Sverdlovsk, USSR, 1975; pp. 58–71. (In Russian)
30. Korobkov, V.F.; Baimagambetov, B.K.; Sapozhnikov, P.K.; Ulukpanov, K.T. *Guidebook of Geological Excursions in the Mugodzhar Mountains*; Aktobe State University Press: Aktobe, Kazakhstan, 2012. (In Russian)
31. Kazantseva, T.T. On the Stratigraphy of the Zilair Series of the Western Slope of the Southern Urals. *Dokl. Akad. Nauk. SSSR* **1970**, *194*, 649–652. (In Russian)
32. Kazantseva, T.T. On the Stratigraphy and Geodynamics of the Zilair Deposits in the Southern Urals. *Izv. Ufim. Nauchnogo Tsentra RAN* **2021**, *3*, 77–88. (In Russian) [CrossRef]
33. Yanshin, A.L. Tectonics of the Kargaly Mountains. *Byulleten MOIP Geol. Ser.* **1932**, *10*, 308–345.
34. Edwards, R.L.; Wasserburg, G.J. The age and emplacement of obducted oceanic crust in the Urals from Sm–Nd and Rb–Sr systematics. *Earth Planet. Sci. Lett.* **1985**, *72*, 389–404. [CrossRef]
35. Downey, M.W.; Morgan, W.A.; Threet, J.C. *Petroleum Provinces of the Twenty-First Century*; American Association of Petroleum Geologists: Tulsa, OK, USA, 2001; 573p.
36. Ingebritsen, S.E.; Manning, C.E. Permeability of the continental crust: Dynamic variations inferred from hydrothermal systems and metamorphism. *Geofluids* **2010**, *10*, 193–205. [CrossRef]
37. Sibson, R.H. Crustal stress, faulting and fluid flow. *Geol. Soc. Lond. Spec. Publ.* **1994**, *78*, 69–84. [CrossRef]
38. Sibson, R.H. Structural permeability of fluid-driven fault-fracture. *J. Struct. Geol.* **1996**, *18*, 1031–1042. [CrossRef]
39. Sibson, R.H. Fluid involvement in normal faulting. *J. Geodyn.* **2000**, *29*, 469–499. [CrossRef]
40. Bense, V.F.; Gleeson, T.; Loveless, S.E.; Bour, O.; Scibek, J. Fault zone hydrogeology: Modeling fluid flow in heterogeneous, fault-controlled hydrothermal systems. *Earth-Sci. Rev.* **2013**, *127*, 171–192. [CrossRef]
41. Siler, D.L.; Pepin, J. 3-D geologic controls of hydrothermal fluid flow at Brady geothermal field, Nevada, USA. *Geothermics* **2021**, *94*, 102112. [CrossRef]
42. Zhang, Y.-G.; Frantz, J.D. Determination of the homogenization temperatures and densities of supercritical fluids in the system $NaClKClCaCl_2H_2O$ using synthetic fluid inclusions. *Chem. Geol.* **1987**, *64*, 335–350. [CrossRef]
43. Nardin, E.; Godderis, Y.; Donnadieu, Y.; Le Hir, G.; Blakey, R.C.; Puceat, E.; Aretz, M. Modeling the early Paleozoic long-term climatic trend. *Geol. Soc. Am. Bull.* **2011**, *123*, 1181–1192. [CrossRef]
44. Joachimski, M.M.; Breisig, S.; Buggisch, W.F.; Talent, J.A.; Mawson, R.; Gereke, M.; Morrow, J.R.; Day, J.; Weddige, K. Devonian climate and reef evolution: Insights from oxygen isotopes in apatite. *Earth Planet. Sci. Lett.* **2009**, *284*, 599–609. [CrossRef]
45. Bodnar, R.J. Revised equation for calculating freezing-point depression of H_2O–NaCl solutions. *Geochim. Cosmochim. Acta* **1993**, *57*, 683–684. [CrossRef]
46. Bodnar, R.J. Introduction to fluid inclusions. In *Fluid Inclusions: Analysis and Interpretation*; Samson, I., Anderson, A., Marshall, D., Eds.; Mineralogical Association of Canada Short Course Series; Mineralogical Association of Canada: Québec City, QC, Canada, 2003; Volume 32, pp. 1–8.
47. Potter, R.W.; Clynne, M.A.; Brown, D.L. Freezing point depression of aqueous sodium chloride solutions. *Econ. Geol.* **1978**, *73*, 284–285. [CrossRef]
48. Steele-MacInnis, M.; Bodnar, R.J.; Naden, J. Numerical model to determine the composition of H_2O–NaCl–$CaCl_2$ fluid inclusions based on microthermometric and microanalytical data. *Geochim. Cosmochim. Acta* **2011**, *75*, 21–40. [CrossRef]
49. Drebushchak, V.A.; Ogienko, A.G.; Yunoshev, A.S. Metastable eutectic melting in the NaCl-H_2O system. *Thermochim. Acta* **2017**, *647*, 94–100. [CrossRef]

50. Roedder, E. Fluid Inclusions. In *Reviews in Mineralogy*; Mineralogical Society of America: Washington, DC, USA, 1984; Volume 12, 644p.
51. Dubois, M.; Ayt Ougougdal, M.; Meere, P.; Royer, J.J.; Boiron, M.C.; Cathelineau, M. Temperature of paleo- to modern self-sealing within a continental rift basin; the fluid inclusion data (Soultz-sous-Forêts, Rhine Graben, France). *Eur. J. Mineral.* **1996**, *8*, 1065–1080.
52. Smith, M.P.; Savary, V.; Yardley, B.W.D.; Valley, J.W.; Royer, J.J.; Dubois, M. The evolution of the deep flow regime at Soultz-sous-Forêts, Rhine Graben, eastern France: Evidence from a composite quartz vein. *J. Geophys. Res.-Part B-Solid Earth* **1998**, *103*, 27223–27237. [CrossRef]
53. Cathelineau, M.; Boiron, M.C. Downward penetration and mixing of sedimentary brines and dilute hot waters at 5 km depth in the granite basement at Soultz-sous-Forêts (Rhine graben, France). *Comptes Rendus Geosci.* **2010**, *342*, 560–565. [CrossRef]
54. Le Carlier, C.; Royer, J.J.; Flores, E.L. Convective heat transfer at the Soultz-sous-Forêts Geothermal Site: Implications for oil potential. *First Break* **1994**, *12*, 553–560. [CrossRef]
55. Dumitru, T.A. Effects of subduction parameters on geothermal gradients in forearcs, with an application to Franciscan Subduction in California. *J. Geophys. Res. Solid Earth* **1991**, *96*, 621–641. [CrossRef]
56. Ernst, W.G. Do mineral parageneses reflect unusually high- pressure conditions of Franciscan metamorphism? *Am. J. Sci.* **1971**, *270*, 81–108. [CrossRef]
57. Ernst, W.G. Tectonic history of subduction zones inferred from retrograde blueschist P-T paths. *Geology* **1988**, *16*, 1081–1084. [CrossRef]
58. Springer, M.; Förster, A. Heat-flow density across the Central Andean subduction zone. *Tectonophysics* **1998**, *291*, 123–139. [CrossRef]
59. Jaupart, C.; Mareschal, J.C. 6.05—Heat Flow and Thermal Structure of the Lithosphere. *Treatise Geophys.* **2007**, *6*, 217–251. [CrossRef]
60. Zhanserkeyeva, A.A.; Kassenov, A.K. Prospect evaluation based on integrated petroleum system analysis: Block E case study, south-eastern edge of Precaspian Basin (Kazakhstan). *J. Pet. Explor. Prod. Technol.* **2022**, *12*, 2625–2642. [CrossRef]
61. Lepezin, G.G.; Travin, A.V.; Yudin, D.S.; Volkova, N.I.; Korsakov, A.V. Age and thermal history of the Maksyutov metamorphic complex: 40Ar/39Ar evidence. *Petrology* **2006**, *14*, 98–114. [CrossRef]
62. Leech, M.L.; Stockli, D.F. The late exhumation history of the ultrahigh-pressure Maksyutov Complex, south Ural Mountains, from new apatite fission track data. *Tectonics* **2000**, *19*, 153–167. [CrossRef]
63. Kukkonen, I.T.; Golovanova, I.V.; Khachay, Y.V.; Druzhinin, V.S.; Kosarev, A.M.; Schapov, V.A. Low geothermal heat flow of the Urals fold belt. *Tectonophysics* **1997**, *276*, 63–85. [CrossRef]
64. Rakhimov, I.R.; Ankusheva, N.N.; Samigullin, A.A.; Shanina, S.N. Origin and Evolution of Ore-Forming Fluids at the Small-Sized Gold Deposits in the Khudolaz Area, Southern Urals. *Minerals* **2023**, *13*, 781. [CrossRef]
65. Korekina, M.A.; Savichev, A.N. Conditions of Formation and Sources of Fluids of Barren Vein Quartz Deposits of Hydrothermal–Metamorphogenic–Metasomatic and Hydrothermal–Metamorphogenic Genesis, Middle and Southern Urals. *Vestn. St. Petersburg Univ. Earth Sci.* **2023**, *68*, 201–216. [CrossRef]
66. Sharipova, A.A.; Michurin, S.V.; Krupenin, M.T.; Garaeva, A.A.; Kanipova, Z.A. Vein Quartz from Gold Occurrences in Riphean Deposits of the Avzyan Ore District, Southern Urals: Mineralogical and Thermocryometric Features. *Bull. Perm Univ. Geol.* **2017**, *16*, 216–230. [CrossRef]